Long non-coding RNA DIO3OS binds to microRNA-130b to restore radiosensitivity in esophageal squamous cell carcinoma by upregulating PAX9

Jun-Qi Liu
The First Affiliated Hospital of Zhengzhou University
Xiang-Xiang Yang
The First Affiliated Hospital of Zhengzhou University
Yue-Xin Guo
The First Affiliated Hospital of Zhengzhou University
Xin Wang
The First Affiliated Hospital of Zhengzhou University
Hao Gu
The First Affiliated Hospital of Zhengzhou University
Song Zhang
The First Affiliated Hospital of Zhengzhou University
Liang Gao
Saarland University
Di Zhao (junq_liu@126.com)
The First Affiliated Hospital of Zhengzhou University
Rui-Tai Fan
The First Affiliated Hospital of Zhengzhou University

Research

Keywords: DIO3OS, MicroRNA-130b, Paired box 9, Radiosensitivity, Esophageal squamous cell carcinoma

Posted Date: November 9th, 2019

DOI: https://doi.org/10.21203/rs.2.17052/v1

Version of Record: A version of this preprint was published at Cancer Gene Therapy on June 28th, 2021.
See the published version at https://doi.org/10.1038/s41417-021-00344-2.

Abstract

Background: Esophageal squamous cell carcinoma (ESCC) ranks as one of the most fatal cancers worldwide for its aggression and unsatisfactory survival rate. The long non-coding RNA (lncRNA)-microRNA (miRNA)-mRNA axis has been highlighted as a potency biomarker for enhancing the radiosensitivity of ESCC. Hence, we investigated the functional mechanism of the DIO3OS/miR-130b/paired box 9 (PAX9) axis in the radioresistance of ESCC cells.

Methods: In cell experiments, we altered the miR-130b expression in ESCC cells using mimics or inhibitors to examine its effects on ESCC cell activities in response to 4 Gy irradiation, as well as the involvement of DIO3OS and PAX9. Tumor xenograft experiments were then conducted to observe the effect of miR-130b, DIO3OS and PAX9 on radiosensitivity of ESCC ells in vivo .

Results: miR-130b was found to be highly-expressed in the ESCC. Downregulated miR-130b inhibited proliferation, invasion and resistance to apoptosis in ESCC cells. DIO3OS and PAX9 were reduced in ESCC. A notable finding revealed that miR-130b could bind to DIO3OS and PAX9 respectively. DIO3OS could upregulate PAX9 by binding to miR-130b, which ultimately promoted the radiosensitivity of ESCC in vitro and in vivo .

Conclusion: Taken together, DIO3OS upregulates the expression of PAX9 by binding to miR-130b, ultimately promoting the radiosensitivity of ESCC. Keywords: DIO3OS. MicroRNA-130b. Paired box 9. Radiosensitivity. Esophageal squamous cell carcinoma.

Background

Esophageal cancer (EC) remains the seventh most common cancer and the sixth highest cause of cancer-related death worldwide in 2018 according to a status report on the global burden of cancer worldwide [1]. Esophageal squamous cell carcinoma (ESCC) is a malignancy characterized by a high rate of morbidity and mortality largely due to the delayed diagnosis in high-grade stages, which has been reported to account for approximately 90% of all the EC cases on an annual basis globally [2]. ESCC is extremely prevalent in the EC belt, from the northern China through central Asia to northern Iran [3]. In Chinese population, EC ranks as the fourth most prevalent malignancy and also the fourth leading cause of cancer-related fatality, resulting in approximately 100 per 100,000 cases diagnosed annually [4]. Multiple studies have demonstrated that the radiochemotherapy and surgery are reasonable choices for patients with ESCC to improve their survival rate [5–7]. Although the advancements in surgical methods and other treatment regimens improve prognosis of ESCC patients, ESCC still remains one of the most lethal cancers with a devastating 5-year survival rate in the advanced stage of less than 15% [8]. It’s worth noting that radiotherapy resistance is one of the most critical causes for local tumor recurrence, distant metastasis or even mortality in cancers, including ESCC [9, 10]. In order to increase overall survival and prevent radioresistance, novel therapies tailored with the aid of molecular biomarkers of ESCC are urgently required.

Previous microarray-based technologies have highlighted circulating microRNAs (miRNAs) as potential molecular biomarkers capable of providing an early diagnosis of ESCC [11]. MiRNAs are able to mediate the gene expression by interacting with their corresponding targets to enhance degradation and/or inhibit translation [12]. The dysregulated expression and promoted stability of miRNAs have been implicated in cases of acquired resistance to existing therapies in various types of cancers, including ESCC [13]. MicroRNA–130b (miR–130b) has been identified to exhibit high expression in ESCC tissues with its overexpression reported to facilitate proliferation, invasion and migration of ESCC cells [14]. Furthermore, overexpressed miR–130b could augment chemoresistance and cell survival of breast cancer cells by binding to phosphatase and tensin homolog (PTEN) [15]. The preliminary microarray analysis performed in the present study identified the binding of miR–130b to differentially expressed long noncoding RNA (lncRNA) DIO3OS and paired box 9 (PAX9) gene, which led to a hypothesis of the involvement of the DIO3OS/miR–130b/PAX9 axis in the radiosensitivity of ESCC. The downregulated DIO3OS expression has been identified in tissue and plasma samples from patients with inflammatory bowel disease [16]. Various lncRNAs have been shown to play critical roles in stimulating or attenuating radiosensitivity in cancers, including LINC00483 in lung adenocarcinoma [17] and POU6F2-AS2 in ESCC [18]. In addition, the abnormally decreased PAX9 expression is associated with the worsening malignancy of cancerous and dysplastic epithelium of the oesophagus [19]. Hence, the central objective of the current study was to investigate the regulatory relationship of the DIO3OS/miR–130b/PAX9 axis and its involvement in the radiosensitivity of ESCC cells.

Materials And Methods

Ethics statement

The *in vivo* study adhering to the ARRIVE guidelines was carried out with the approval of the Ethics Committee of The First Affiliated Hospital of Zhengzhou University (ID: 201311005).

Cell culture

Five ESCC cell lines (EC109, TE–1, KYSE70, KYSE270, and KYSE30) and human normal esophageal epithelial cells (HEEC) were purchased from the American Type Culture Collection (Manassas, VA, USA). All cell lines were exposed to low sugar Dulbecco's modified eagle medium (DMEM) containing 10% fetal bovine serum (FBS, Gibco, Grand Island, NY, USA) and incubated at 37°C with 5% CO_2 and 95% saturated humidity. The cells were passaged after cell confluence had reached approximately 90%.

Cell treatment

The ESCC cells were treated with 4 Gy radiation and transfected with miR–130b inhibitor, miR–130b mimic, oe-DIO3OS, wild type (wt)-DIO3OS, mutant (mut)-DIO3OS, wt-PAX9 and mut-PAX9. The target plasmid, mimic and inhibitor of miR–130b were obtained from Dharmacon (Lafayette, CO, USA). Cell

density was adjusted based on the cell growth rate, after which the cells were cultured in a 6-well plate to make the cells reach a confluence of 80% - 90% for transfection on the next day. Transfection was performed using a lipofectamine 2000 (Invitrogen, Carlsbad, CA, USA) kit. Opti-MEM medium (250 μL, Gibco, Grand Island, NY, USA) was utilized to dilute 4 μg target plasmid and 10 μL lipofectamine 2000, with the diluents mixed together in a uniform manner after allowed to stand at room temperature for 5 min. After 20 min, the mixed solution of lipofectamine 2000 and plasmid was supplemented into the wells. After 8 h, the cells were cultured again in a fresh medium for 48 h.

RNA isolation and quantification analysis

Total RNA was isolated using a RNeasy Mini Kit (Qiagen, Valencia, CA, USA), with the RNA subsequently synthesized into complementary DNA (cDNA) using a reverse transcription kit (RR047A, Takara, Tokyo, Japan). The reverse transcription was performed at 37°C for 30 min and at 85°C for 5 s in a 20 μL reaction volume. The sample was then loaded using SYBR Premix EX Taq kit (RR420A, Takara, Tokyo, Japan) and subjected to reverse transcription quantitative polymerase chain reaction (RT-qPCR) using a real-time PCR instrument (ABI7500, ABI, Foster City, CA, USA). Primers used in this study are depicted in Table 1 and were designed and synthesized by Sangon Biotech Co., Ltd. (Shanghai, China). The expression of each miRNA was normalized to glyceraldehyde–3-phosphate dehydrogenase (GAPDH) or U6 and the data were analyzed using the $2^{-\Delta\Delta Ct}$ method: $\Delta\Delta Ct = (\Delta Ct_{\text{target gene}} - \Delta Ct_{\text{housekeeping gene}})_{\text{the experimental group}} - (\Delta Ct_{\text{target gene}} - \Delta Ct_{\text{housekeeping gene}})_{\text{the control group}}$.

Protein isolation and quantification analysis

The cells were lysed with radioimmunoprecipitation assay (RIPA) lysis buffer supplemented with phenylmethanesulfonyl fluoride (PMSF) in order to harvest total protein. The bicinchoninic acid (BCA) kit was used to quantify the protein concentration of each cell lysate. The protein (50 μg) was run on sodium dodecyl sulfate-polyacrylamide gel electrophoresis and subsequently transferred onto a polyvinylidene fluoride (PVDF) membrane. The membranes were blocked using 5% skim milk powder at room temperature for 1 h and probed overnight at 4°C with diluted primary antibodies specific for PAX9 (ab151570, 1: 1000), Ki67 (ab92742, 1: 1000), cleaved caspase–3 (ab2302, 1: 1000), and GAPDH (ab9485, 1: 2500). The membranes were then incubated with horseradish peroxidase (HRP)-labeled goat anti-rabbit secondary antibody specific for immunoglobulin G (IgG) (H + L) (ab97051, 1: 2000) for 1 h. All the aforementioned antibodies were purchased from Abcam company (Cambridge, UK). GAPDH was used as the loading control. Finally, the images of protein bands were captured with a Bio-Rad image analysis system (Bio-Rad, Hercules, CA, USA) using an enhanced chemiluminescence (ECL) detection kit (Cat. No. BB–3501, Amersham, Little Chalfont, Buckinghamshire, UK). Densitometric analysis of protein bands was performed using Quantity One v4.6.2 software.

RNA immunoprecipitation (RIP)

The cultured cells were lysed and mixed using 50 μL of magnetic beads. The mixture was then vortexed following the addition of 0.5 mL RIP wash buffer (EHJ-BVIS08102, Xiamen Huijia Biotechnology Co., Ltd., Xiamen, China), and placed in the magnetic separator for the gathering of magnetic beads. The collected magnetic beads were resuspended by 100 μL RIP Wash Buffer. Next, 5 μg Ago2 antibody (P10502500, Otwo Biotech Inc. Shenzhen, Guangdong, China) was spun down for 30 min at room temperature, with normal mouse IgG regarded as the NC. The magnetic bead-antibody mixture was supplemented with 900 μL RIP immunoprecipitation buffer (P10403138, Otwo Biotech Inc.) After centrifugation, the supernatant (100 μL) was inserted into the tube with magnetic bead-antibody mixture, with 1 mL taken as the final volume of the immunoprecipitation reaction, followed by vortexing at 4°C overnight. The magnetic beads were then washed 6 times and incubated with 150 μL proteinase K buffer at 55°C for 30 min for RNA purification. The RNA was then extracted using a conventional TRIZOL method, followed by RT-qPCR detection.

Dual luciferase reporter gene assay

The wt-DIO3OS, mut-DIO3OS, wt-PAX9–3'UTR and mut-PAX9–3'UTR were designed and provided by Shanghai GenePharma Co., Ltd. (Shanghai, China). Mimic NC and miR–130b mimic were separately co-transfected with wt-DIO3OS, mut-DIO3OS, wt-PAX9–3'UTR, and mut-PAX9–3'UTR to EC109 cells. The luciferase activities in the indicated cells were determined using a Promega GLomax 20/20 luminometer (E5311, Shaanxi Zhongmei Biotechnology Co., Ltd., Shaanxi, China) 48 h after transfection according to the manufacturer's instructions of Genecopoeia dual luciferase assay kit (D0010, Solarbio Technology Co., Ltd., Beijing, China).

Fluorescence in situ hybridization (FISH)

FISH assay was employed to identify the subcellular localization of DIO3OS in accordance with the instructions of the Ribo^{TM} lncRNA FISH Probe Mix (Red) (C10920, Guangzhou RiboBio Co., Ltd. (Guangzhou, Guangdong, China). The cells were seeded (at 6×10^4 cells/well) in 24-well culture plates to achieve a cell confluence of 60% - 70%. The cells were subsequently fixed with 1 mL 4% paraformaldehyde at room temperature for 10 min. Next, cells in each well was allowed to stand with 1 mL pre-cooled permeabilization solution (PBS containing 0.5% Triton X–100) at 4°C for 5 min. Next, the cells were sealed by 200 μL pre-hybridization solution per well for 30 min at 37°C. Following removal of the pre-hybridization solution, the cells were incubated with pre-hybridization solution containing anti-DIO3OS nucleotide probe (GeneCreate Biotech., Wuhan, Hubei, China) overnight at 37°C under conditions void of light. Next, after being stained in 4',6-diamidino–2-phenylindole (DAPI) (1: 800) for 10 min, five different fields of view in the cells were randomly chosen for fluorescence microscopic observation (Olympus, Tokyo, Japan).

Transwell assay

The apical Transwell chambers (3413, Unique Biotechnology Co. Ltd, Beijing, China) were coated with Matrigel (40111ES08, Yeasen Company, Shanghai, China) diluted at a ratio of 1:8 with pre-cooled serum-free DMEM and incubated at 37°C for 4 - 5 h. Cells at a concentration of 1×10^6 cells/mL were seeded in the chambers. The basolateral chamber was filled with 500 μL DMEM supplemented with 20% FBS, with 3 replicate wells set in each group. After a 24 h period of incubation at 37°C with 5% CO_2, the cells on the upper surface of the transwell chamber were fixed with 5% glutaraldehyde at 4°C and stained with 0.1% crystal violet for 5 min. Five different fields (200 ×) were randomly selected for observation and photography under an inverted fluorescence microscope (TE2000, Nikon Co., Tokyo, Japan). The cells that invaded to the basolateral chamber were counted and analyzed.

Cell counting kit–8 (CCK–8) assay

The cells were seeded into a 96-well plate at a density of 2×10^3 cells each well. A blank control well was set for zero calibration, in which only the cell-free medium was added. In terms of the survival conditions of cells after radiation treatment, the cells transfected for 24 h were exposed to 4 Gy dose X-ray. At the 0^{th}, 24^{th}, 48^{th} and 72^{nd} after irradiation, 10 μL CCK–8 solution was added to each well for another 2-h incubation at 37°C. The optical density (OD) value at 450 nm was determined using a microplate reader (Bio-Rad, Hercules, CA, USA).

Colony formation assay

A total of 1×10^6 cells was placed into a fresh 6-well plate. After 24 h of transfection, the cells were irradiated with X-ray at a dosage of 4 Gy, followed by incubation for 14 days at 37°C with 5% CO_2. Next, the cells were stained with crystal violet for 3 min after immobilization in methanol for 5 min. The number of colonies with more than 50 cells was counted by microscopic inspection. Plating efficiency (PE) = number of clones formed by cells after irradiation/number of cells inoculated. Survival fraction (SF) = PE of cells irradiated at a specific dose/PE of cells irradiated at 0 Gy.

Flow cytometry

The cells (1×10^6 cells/well) were seeded into a 6-well plate. After a 24 h period of transfection, the cells were treated with 4 Gy of radiation. The cells were collected after 24 h of irradiation and detected using an Annexin-V fluorescein isothiocyanate (FITC)-propidium iodide (PI) apoptosis kit (Invitrogen, Carlsbad, CA, USA) and analyzed using a FACScalibur flow cytometry (BD Biosciences, San Jose, CA, USA).

Tumor formation in nude mice

Totally, 72 male or female BALA/C nude mice (Experimental Animal Center of Zhengzhou University), aged 4 weeks and weighing 18 - 25 g, were randomly treated with 4 Gy radiation and delivered with the lentivirus (LV-sh-miR–130b, LV-oe-miR–130b, LV-oe-DIO3OS and LV-oe-PAX9). The lentiviral particles were from GenePharma (Shanghai, China). Tumors were generated by subcutaneously injection into the right abdomen of nude mice with 1×10^6 stably transfected EC109 cells. When the xenograft tumor volumes reached an average volume of about 300 mm^3, the mice were irradiated with 4 Gy of X-ray once a week. The tumor volume was regularly determined every 3 days following irradiation, and volumes were calculated using the formula: $1/2 \times \text{length} \times \text{width}^2$. On the 21st day after the first irradiation, the nude mice were euthanized by carbon dioxide asphyxiation and the tumor was excised for subsequent experiments.

Immunohistochemistry

The sections were baked in a 60°C incubator for 1 h, treated with xylene, and hydrated through a sequence of decreasing concentrations of ethanol. The sections were then incubated for 20 min at room temperature with PBS containing 0.5% Triton. After 2 min of antigen retrieval, the cells were boiled in 0.01 M citrate buffer (pH = 6.0) at 95°C for 20 min. The exogenous peroxidase activity was quenched with 3% H_2O_2 for 15 min. The sections were incuabted with 3% bovine serum albumin (BSA) blocking solution at 37°C for 20 - 30 min, followed by an incubation with diluted primary rabbit anti-human antibodies specific for Ki67 (ab92742, 1: 500) or cleaved caspase–3 (ab2302, 1: 200) at 37°C for 2 h and then with HRP-labeled secondary goat anti-rabbit antibody specific for IgG (ab6721, 1: 1000) at 37°C for 30 min. The above antibodies were from Abcam company (Cambridge, UK). Subsequently, hematoxylin (Shanghai Fusheng Industrial Co., Ltd., Shanghai, China) was used to counter stain nuclei at room temperature for 4 min. Finally, all sections were mounted with 10% glycerol/PBS and observed under a microscope. The immunohistochemistry results were scored in an independent manner using a double-blind method.

Statistical analysis

All statistical analyses from at least three separate experiments were performed using SPSS 21.0 software (IBM Corp, Armonk, NY, USA). Measurement data were presented as mean ± standard deviation. An independent sample *t* test was applied for comparisons between two groups, while one-way analysis of variance (ANOVA) followed by Tukey's post hoc test was adopted for comparison between multiple groups. Comparison at different time points was analyzed using repeated measures ANOVA. Differences that produced *p* values less than 0.05 were accepted as significant.

Results

miR–130b is upregulated in ESCC

Initially, a miRNA microarray was analyzed in order to plot the heatmap of the first 10 differentially expressed miRNAs of GSE97049 and GSE43732 expression profiles from the Gene Expression Omnibus (GEO) database. As depicted in Fig. 1A and Fig. 1B, the expression of hsa-miR−130b−3p was identified to be higher in ESCC tissues than that in the normal tissues. RT-qPCR was subsequently applied to detect the expression of miR−130b in ESCC cell lines (EC109, TE−1, KYSE70, KYSE270, and KYSE30) and human normal esophageal epithelial cells (HEEC) (Fig. 1C). Relative to the expression in HEEC cell line, the miR−130b expression was promoted in the aforementioned five human ESCC cell lines ($p < 0.05$). Notably, the EC109 and KYSE270 cell lines exhibited the highest expression of miR−130b, and were subsequently selected for further experiments. Therefore, miR−130b expressed highly in ESCC.

miR−130b potentiates cell proliferation and invasion and represses apoptosis of ESCC cells

To further define the potential biological significance of miR−130b on ESCC, a series of phenotypic experiments were performed in in ESCC cell lines EC109 and KYSE270 with altered miR−130b expression through treatments with mimic-NC, miR−130b mimic, inhibitor-NC, or miR−130b inhibitor.

The efficiency of miR−130b mimic or inhibitor was measured by RT-qPCR (Fig. 2A), which revealed that the efficiency of miR−130b mimic or inhibitor in EC109 cells reached the prerequisites required for further experiments ($p < 0.05$). The proliferation and invasion of EC109 cells were assessed by CCK−8 and Transwell assays (Fig. 2B-C), which indicated that the cell proliferation and number of invasive cells were reduced in the presence of miR−130b inhibitor when compared with treatment of inhibitor NC ($p < 0.05$) with increases detected in response to miR−130b mimic relative to treatment of mimic-NC ($p < 0.05$). According to flow cytometry (Fig. 2D), the apoptosis rate was enhanced in the presence of miR−130b inhibitor ($p < 0.05$) and decreased following treatment of miR−130b mimic relative to the matched controls ($p < 0.05$). Next, Western blot analysis was carried out to examine the expression of proliferation-, invasion- and apoptosis-related factors (Ki67, MMP−2 and Bax) (Fig. 2E). Treatment with miR−130b inhibitor was found to diminish the expression of Ki67 and MMP−2 and increase that of Bax ($p < 0.05$), while treatment with miR−130b mimic achieved contrasting results ($p < 0.05$). Moreover, identical results were observed in the KYSE270 cells (Supplementary Fig. 1). These outcomes suggested that miR−130b facilitated the proliferation and invasion whereas inhibited the apoptosis of ESCC cells, and its downregulation could reverse these effects.

DIO3OS upregulates the expression of PAX9 by binding to miR−130b

In order to clarify the mechanisms by which miR−130b might participate in ESCC, its target genes were predicted in RNA22, miRWalk and DIANA. The Venn map (Fig. 3A) was plotted based on the comparison between the predicted results and the differentially expressed genes obtained from GSE20347, GSE77861

and GSE23400 from the GEO database, which found two intersected genes EMP1 and PAX9. Thus, it could be inferred that the differential expression of these two genes in ESCC could be regulated by miR–130b. Hence, in order to corroborate this hypothesis, the function of miR–130b on expression of EMP1 and PAX9 was tested by RT-qPCR (Fig. 3B), which indicated that only the expression of PAX9 was affected ($p < 0.05$). Moreover, a decrease in the expression of PAX9 has been linked to human esophageal dysplasia and cancerous epithelial malignancy [19]. The expression of PAX9 in GSE20347, GSE77861 and GSE23400 is illustrated in Fig. 3C, whereby we suggested that miR–130b may target PAX9 and influence the development of ESCC. The RT-qPCR detection (Fig. 3D) demonstrated that PAX9 was downregulated in both ESCC cells ($p < 0.05$). The putative binding sites of miR–130b and PAX9 were predicted by biological website and further substantiated by dual luciferase reporter gene assay (Fig. 3E). The transfection of both miR–130b mimic and wt-PAX9–3'UTR resulted in a marked decline in luciferase activity ($p < 0.05$), while no significant difference in relation to the luciferase activity was found in co-transfection of miR–130b mimic and mut-PAX9–3'UTR ($p > 0.05$).

Next, the upstream regulatory mechanism of miR–130b was investigated through bioinformatic analysis, and the lncRNAs binding to miR–130 were predicted through RAID and RNA22 databases. The comparison between the predicted results and the differentially expressed lncRNAs obtained from GSE45670 and GSE45168 only identified one intersection, lncRNA DIO3OS (Fig. 3F). In addition, the GSE45670 and GSE45168 datasets demonstrated that DIO3OS was abnormally lowly expressed in ESCC (Fig. 3G). According to aforementioned results, we subsequently asserted the hypothesis that DIO3OS may affect the occurrence and development of ESCC by binding to miR–130b that targeted PAX9. The downregulation of DIO3OS in ESCC cells was confirmed by RT-qPCR ($p < 0.05$, Fig. 3H). The expression of DIO3OS and PAX9 in 161 cases of ESCC tissue in the Cancer Genome Atlas (TCGA) database was analyzed, with a positive correlation detected between their expressions (Fig. 3I).

Moreover, miR–130b was found to negatively regulate the expression of DIO3OS and PAX9 in cell experiments (Fig. 3J). The binding relationship of miR–130b and DIO3OS were predicted by biological website and further corroborated by dual luciferase reporter gene assay (Fig. 3K). The co-transfection of miR–130b mimic and wt-DIO3OS resulted in a decrease in luciferase activity ($p < 0.05$), while no significant difference was detected in terms of luciferase activity in the co-transfection of miR–130b mimic and mut-DIO3OS ($p > 0.05$). Next, to investigate the effect of DIO3OS and miR–130b on PAX9 expression in ESCC, the EC109 cells were transfected with oe-DIO3OS and miR–130b mimic alone or in combination. RT-qPCR detected PAX9 expression in EC109 cells. It was found that PAX9 expression was restored by oe-DIO3OS and mimic NC, but decreased by the treatment of oe-DIO3OS and miR–130b mimic when compared with relative controls ($p < 0.05$) (Fig. 3L). Next, in order to further elucidate the potential function of DIO3OS as a mediator of miR–130b to regulate PAX9, EC109 cells were also treated with oe-DIO3OS and miR–130b mimic either separately or in combination. Dual luciferase reporter gene assay revealed that the treatment of oe-DIO3OS elevated the luciferase activity of wt-PAX9 3'-UTR ($p < 0.05$), which could be reversed following the combined treatment of oe-DIO3OS and miR–130b mimic (Fig. 3M). RIP assay indicated that the enrichment of miR–130b, DIO3OS and PAX9 after the treatment of anti-Ago2 was increased ($p < 0.05$) (Fig. 3N). Finally, the cellular localization of DIO3OS expression in

EC109 cells by RNA-FISH indicated that DIO3OS was predominately expressed in the cytoplasm of the EC109 cells (Fig. 3O). Hence, the aforementioned results further confirmed that DIO3OS could bind to miR−130b to regulate PAX9.

DIO3OS and PAX9 reverse the effect of miR−130b on sensitivity of ESCC to radiotherapy

In order to further verify the role of miR−130b in the radiosensitivity in ESCC cells, EC109 and KYSE270 cells were irradiated with 4 Gy X-ray and transfected with oe-DIO3OS, miR−130b mimic and oe-PAX9. The transfection efficiency reached the requirements for further experimentation ($p < 0.05$), based on RT-qPCR evaluation (Fig. 4A). The survival ability of the cells was examined by CCK−8 assay and colony formation assay (Fig. 4B-C). In response to 4 Gy radiation, the survival ability was enhanced in ESCC cells treated with miR−130b mimic + oe-NC ($p < 0.05$), and attenuated in those transfected with miR−130b mimic + oe-PAX9 ($p < 0.05$). No profound difference was observed in the survival ability of the ESCC cells treated with miR−130b mimic + oe-DIO3OS in response to 4 Gy radiation ($p > 0.05$). The survival ability of the ESCC cells treated with miR−130b mimic + oe-DIO3OS and those with miR−130b mimic + oe-PAX9 were hindered when compared with that of the cells treated with miR−130b mimic + oe-NC in response to 4 Gy radiation ($p < 0.05$). The apoptosis of ESCC cells was assessed by flow cytometry (Fig. 4D). In the presence of 4 Gy radiation, the transfection of miR−130b mimic + oe-NC lowered the apoptosis rate of ESCC cells ($p < 0.05$), while the treatment of miR−130b mimic + oe-PAX9 exhibited an elevated rate of apoptosis ($p < 0.05$), with no difference regarding the rate of apoptosis identified with the transfection of 4 Gy + miR−130b mimic + oe-DIO3OS ($p > 0.05$). An increase in the apoptosis rate was detected in the ESCC cells receiving 4 Gy radiation with the transfection of miR−130b mimic + oe-DIO3OS and transfection of miR−130b mimic + oe-PAX9 versus the transfection of miR−130b mimic + oe-NC ($p < 0.05$). The expression of PAX9, Ki67 and cleaved caspase−3 was assessed by Western blot analysis (Fig. 4E). Increased Ki67 expression and reduced expression of PAX9 and cleaved caspase−3 were determined in the ESCC cells irradiated by 4 Gy X-rays and treated with miR−130b mimic + oe-NC ($p < 0.05$), while an opposite trend was observed in those irradiated by 4 Gy X-rays and treated with miR−130b mimic + oe-PAX9 ($p < 0.05$). Additionally, the presence of miR−130b mimic + oe-DIO3OS resulted in no significant difference in relation to the expression of PAX9, Ki67 and cleaved caspase−3 in response to 4 Gy radiation ($p > 0.05$). Following 4 Gy radiation, the ESCC cells showed decreased Ki67 expression and enhanced expression of PAX9 and cleaved caspase−3 in the presence of miR−130b mimic + oe-DIO3OS and miR−130b mimic + oe-PAX9 versus the presence of miR−130b mimic + oe-NC ($p < 0.05$). Identical results were obtained in the KYSE270 cells (Supplementary Fig. 2). All these data demonstrated that the effect of miR−130b on radiosensitivity in ESCC could be reversed by DIO3OS or PAX9.

DIO3OS and PAX9 overturn the effect of miR−130b on radiosensitivity of ESCC in vivo

In order to further comprehend the effects associated with the DIO3OS/miR−130b/PAX9 axis on the radiosensitivity of ESCC *in vivo,* a series of experiments were conducted in nude mice treated with LV-sh-

miR−130b, LV-oe-miR−130b, LV-oe-DIO3OS and LV-oe-PAX9 alone or in combination in response to 4 Gy radiation. The volume and weight of the transplanted tumor were diminished in the presence of 4 Gy radiation + LV-sh-miR−130b ($p < 0.05$), while elevated in the presence of 4 Gy radiation + LV-oe-miR−130b ($p < 0.05$). Meanwhile, when compared to the treatment of 4 Gy + LV-oe-miR−130b, the volume and weight of the transplanted tumor decreased in the presence of 4 Gy + LV-oe-miR−130b + LV-oe-DIO3OS and 4 Gy + LV-oe-miR−130b + LV-oe-PAX9 (Fig. 5A-B). Then Ki67, cleaved caspase−3 and PAX9 expression in the transplanted tumors was examined by Western blot analysis (Fig. 5C). The treatment of 4 Gy radiation + LV-sh-miR−130b led to reduction in the expression of Ki67 along with a heightened expression of cleaved caspase3 and PAX9 ($p < 0.05$), while treatment with 4 Gy radiation + LV-oe-miR−130b led to opposite results ($p < 0.05$). Besides, the treatment of 4 Gy + LV-oe-miR−130b + LV-oe-DIO3OS and 4 Gy + LV-oe-miR−130b + LV-oe-PAX9 resulted in weakened expression of Ki67 and strengthened expression of cleaved caspase3 and PAX9 when compared with the treatment of 4 Gy + LV-oe-miR−130b ($p < 0.05$). Furthermore, the Ki67 and cleaved caspase3 positive expression in transplanted tumors was observed by immunohistochemistry (Fig. 5D). The expression of Ki67 was diminished, and that of cleaved caspase3 was increased in the presence of 4 Gy radiation + LV-sh-miR−130b ($p < 0.05$), while an opposite trend was identified following treatment of 4 Gy radiation + LV-oe-miR−130b ($p < 0.05$). Moreover, in contrast to the treatment of 4 Gy + LV-oe-miR−130b, the treatment of 4 Gy + LV-oe-miR−130b + LV-oe-DIO3OS and 4 Gy + LV-oe-miR−130b + LV-oe-PAX9 downregulated the expression of Ki67 and upregulated expression of cleaved caspase3 ($p < 0.05$). All these findings suggested that the effect of miR−130b on radiosensitivity of ESCC cells could be reversed by DIO3OS or PAX9.

Discussion

ESCC is widely known to have a poor survival rate, largely due to its aggressive invasion, metastasis and resistance of tumor cells to chemotherapy or/and radiotherapy [1]. Stimulatingly, the importance of the lncRNA-miRNA-mRNA interaction has been highlighted in radiosensitivity of cancers, including cervical squamous cell carcinoma and prostate cancer [20, 21]. Thus, the establishment of new non-invasive biomarkers with lncRNA-miRNA-mRNA interaction of radiosensitivity or radioresistance for ESCC remains instantly required. Hence, the current study was set out to elucidate the role of the DIO3OS/miR−130b/PAX9 axis in ESCC, with our key findings indicating that overexpression of DIO3OS enhanced radiosensitivity of ESCC cells by binding to miR−130b to upregulate PAX9 (Fig. 6).

The microarray-based analysis predicted that miR−130b was overexpressed in ESCC, which was further validated by subsequent detection in ESCC tissue and cell. Moreover, we identified correlation between high expression of miR−130b and a low survival rate in ESCC patients. Identifying the miRNA expression profiles aids in assessing the respective histology of EC and discriminating normal tissue from cancerous tissue [22]. The hsa-miR−130b is considerably elevated in EC and has been reported to be associated with poor EC prognosis [23]. A previous study has documented that miR−130b acts as an oncogenic miRNA in ESCC by targeting and inhibiting the expression of PTEN [14]. Besides, the upregulation of miR−130b−5p has been demonstrated to facilitate the proliferation, migration and colony formation and invasion abilities of gastric cancer cells [24]. During the present study, the *in vitro* experiments in EC109

cells revealed that the overexpression of miR–130b could accelerate the proliferation and invasion and diminish the apoptosis of ESCC cells.

Notably, a series of assays confirmed that DIO3OS upregulated the expression of PAX9 by binding to miR–130b. The interactive effect is one of the most typical methods by which lncRNAs exert their effects. LncRNAs are capable of directly binding to miRNAs, which results in the inhibition of the direct influence of miRNA on downstream genes [25]. For example, lncRNA-p21 has been shown to possess the ability to enhance the protein level of PTEN by acting as an endogenous mediator to directly bind to miR–130b to decrease miR–130b expression [26]. The aforementioned finding was consistent with the results of the current study whereby miR–130b was found to target and negatively regulate the PAX9 gene, while DIO3OS was found to bind to and inhibit the expression of miR–130b. The expression of PAX9 was diminished by miR–130b, an effect of which could be restored by DIO3OS.

In order to ascertain the roles of miR–130b on the radiosensitivity of ESCC cells, the ESCC cells were irradiated with 4 Gy X-rays after different transfection. The results obtained demonstrated that overexpression of DIO3OS could reverse the effect exerted by miR–130b on the radiosensitivity of ESCC by elevating the expression of PAX9. MiRNAs in addition to other non-coding RNAs have been highlighted as promising targets for the development of future anticancer drugs [27]. For example, the deficiency of miR–130b triggers a marked reduction in chemoresistance *via* the PTEN-PI3K/Akt signaling pathway in breast cancer MCF–7 cells [15]. LncRNA DIO3OS has been emphasized as a novel promising biomarker for the diagnosis of inflammatory bowel disease [16]. Interestingly, PAX9 has been established to modulate the differentiation of squamous cells and carcinogenesis in oro-oesophageal epithelium [28]. Additionally, PAX9 has been highlighted as a key player in the differentiation process of esophageal keratinocytes and internal stratified squamous epithelium [19]. The prognostic value of PAX9 in radiosensitivity has been identified, and ESCC patients with high PAX9 expression have a more favorable 5-year disease-free survival [29]. Lee et al. asserted that inhibition of PAX9 induces apoptosis in oral squamous cell carcinoma cells and attenuates the cancer cell survival [30]. Hence, those findings provided evidence that the radioresistance of ESCC cells enhanced by upregulated miR–130b could be inhibited by overexpression of DIO3OS and PAX9.

Conclusions

The findings of the current study support the position that the DIO3OS/miR–130b/PAX9 axis is a promising novel biomarker in the radiotherapy of ESCC. Our study has provided evidence suggesting that lncRNA DIO3OS promotes the expression of the tumor suppressor PAX9 by binding to miR–130b, which ultimately elevates ESCC cell radiosensitivity. However, whether the therapeutic target is appropriate to human beings requires further verification. Also, our research is still a preliminary one, indicating more experiments in this filed are required in the future. We also recognize that other mechanisms maybe in place to regulate such an axis, which warrants explorations in the future.

Abbreviations

ESCC: Esophageal squamous cell carcinoma; lncRNA: long non-coding RNA; miRNA: microRNA; PAX9: paired box 9; EC: Esophageal cancer; miR–130b: MicroRNA–130b; PTEN: phosphatase and tensin homolog; HEEC: human normal esophageal epithelial cells; FBS: fetal bovine serum; cDNA: complementary DNA; RIPA: radioimmunoprecipitation assay; PMSF: phenylmethanesulfonyl fluoride; BCA: bicinchoninic acid; PVDF: polyvinylidene fluoride; ECL: enhanced chemiluminescence; RIP: RNA immunoprecipitation; FISH: Fluorescence in situ hybridization; DAPI: 4',6-diamidino–2-phenylindole; CCK–8: Cell counting kit–8; OD: optical density; PE: Plating efficiency; SF: Survival fraction; FITC: fluorescein isothiocyanate; BSA; bovine serum albumin; ANOVA: analysis of variance; GEO: Gene Expression Omnibus.

Declaration

Acknowledgments

We would like extend our sincere appreciation to the reviewers for their critical comments on this article.

Authors' contributions

Jun-Qi Liu, Xiang-Xiang Yang and Yue-Xin Guo designed the study. Xin Wang, Hao Gu, Song Zhang and Liang Gao collated the data, carried out data analyses and produced the initial draft of the manuscript. Jun-Qi Liu, Di Zhao and Rui-Tai Fan contributed to drafting the manuscript. All authors have read and approved the final submitted manuscript.

Funding

None.

Availability of data and materials

All data in this article is available.

Ethics approval and consent to participate

The *in vivo* study adhering to the ARRIVE guidelines was carried out with the approval of the Ethics Committee of The First Affiliated Hospital of Zhengzhou University (ID: 201311005).

Consent for publication

Not applicable.

Competing interests

The authors declare that they have no competing interests.

Author details

[1] Department of Radiotherapy, The First Affiliated Hospital of Zhengzhou University, Zhengzhou 450000, P. R. China. [2] Center of Experimental Orthopaedics, Saarland University, Homburg, Germany; Kirrberger Strasse, Building 37, D–66421 Homburg, Germany. [3] Department of Endocrinology, The First Affiliated Hospital of Zhengzhou University, Zhengzhou 450000, P. R. China

References

1.Bray F, Ferlay J, Soerjomataram I, Siegel RL, Torre LA, Jemal A. Global cancer statistics 2018: GLOBOCAN estimates of incidence and mortality worldwide for 36 cancers in 185 countries. CA Cancer J Clin. 2018;68:394–424.

2.Abnet CC, Arnold M, Wei WQ. Epidemiology of Esophageal Squamous Cell Carcinoma. Gastroenterology. 2018;154:360–73.

3.Lin Y, Totsuka Y, He Y, Kikuchi S, Qiao Y, Ueda J, Wei W, Inoue M, Tanaka H. Epidemiology of esophageal cancer in Japan and China. J Epidemiol. 2013;23:233–42.

4.Domper Arnal MJ, Ferrandez Arenas A, Lanas Arbeloa A. Esophageal cancer: Risk factors, screening and endoscopic treatment in Western and Eastern countries. World J Gastroenterol. 2015;21:7933–43.

5.Smyth EC, Lagergren J, Fitzgerald RC, Lordick F, Shah MA, Lagergren P, Cunningham D. Oesophageal cancer. Nat Rev Dis Primers. 2017;3:17048.

6.Pottgen C, Stuschke M. Radiotherapy versus surgery within multimodality protocols for esophageal cancer—a meta-analysis of the randomized trials. Cancer Treat Rev. 2012;38:599–604.

7.Gebski V, Burmeister B, Smithers BM, Foo K, Zalcberg J, Simes J, Australasian Gastro-Intestinal Trials G. Survival benefits from neoadjuvant chemoradiotherapy or chemotherapy in oesophageal carcinoma: a meta-analysis. Lancet Oncol. 2007;8:226–34.

8.Pennathur A, Farkas A, Krasinskas AM, Ferson PF, Gooding WE, Gibson MK, Schuchert MJ, Landreneau RJ, Luketich JD. Esophagectomy for T1 esophageal cancer: outcomes in 100 patients and implications for endoscopic therapy. Ann Thorac Surg. 2009;87:1048–54; discussion 54–5.

9.Ding M, Zhang E, He R, Wang X. Newly developed strategies for improving sensitivity to radiation by targeting signal pathways in cancer therapy. Cancer Sci. 2013;104:1401–10.

10.Su H, Lin F, Deng X, Shen L, Fang Y, Fei Z, Zhao L, Zhang X, Pan H, Xie D, et al. Profiling and bioinformatics analyses reveal differential circular RNA expression in radioresistant esophageal cancer cells. J Transl Med. 2016;14:225.

11.Zheng D, Ding Y, Ma Q, Zhao L, Guo X, Shen Y, He Y, Wei W, Liu F. Identification of Serum MicroRNAs as Novel Biomarkers in Esophageal Squamous Cell Carcinoma Using Feature Selection Algorithms. Front Oncol. 2018;8:674.

12.Bartel DP. MicroRNAs: genomics, biogenesis, mechanism, and function. Cell. 2004;116:281–97.

13.Malhotra A, Sharma U, Puhan S, Chandra Bandari N, Kharb A, Arifa PP, Thakur L, Prakash H, Vasquez KM, Jain A. Stabilization of miRNAs in esophageal cancer contributes to radioresistance and limits efficacy of therapy. Biochimie. 2019;156:148–57.

14.Yu T, Cao R, Li S, Fu M, Ren L, Chen W, Zhu H, Zhan Q, Shi R. MiR–130b plays an oncogenic role by repressing PTEN expression in esophageal squamous cell carcinoma cells. BMC Cancer. 2015;15:29.

15.Miao Y, Zheng W, Li N, Su Z, Zhao L, Zhou H, Jia L. MicroRNA–130b targets PTEN to mediate drug resistance and proliferation of breast cancer cells via the PI3K/Akt signaling pathway. Sci Rep. 2017;7:41942.

16.Wang S, Hou Y, Chen W, Wang J, Xie W, Zhang X, Zeng L. KIF9AS1, LINC01272 and DIO3OS lncRNAs as novel biomarkers for inflammatory bowel disease. Mol Med Rep. 2018;17:2195–202.

17.Yang QS, Li B, Xu G, Yang SQ, Wang P, Tang HH, Liu YY. Long noncoding RNA LINC00483/microRNA–144 regulates radiosensitivity and epithelial-mesenchymal transition in lung adenocarcinoma by interacting with HOXA10. J Cell Physiol. 2019;234:11805–21.

18.Liu J, Sun X, Zhu H, Qin Q, Yang X, Sun X. Long noncoding RNA POU6F2-AS2 is associated with oesophageal squamous cell carcinoma. J Biochem. 2016;160:195–204.

19.Gerber JK, Richter T, Kremmer E, Adamski J, Hofler H, Balling R, Peters H. Progressive loss of PAX9 expression correlates with increasing malignancy of dysplastic and cancerous epithelium of the human oesophagus. J Pathol. 2002;197:293–7.

20.Song J, Ye A, Jiang E, Yin X, Chen Z, Bai G, Zhou Y, Liu J. Reconstruction and analysis of the aberrant lncRNA-miRNA-mRNA network based on competitive endogenous RNA in CESC. J Cell Biochem. 2018;119:6665–73.

21.He JH, Han ZP, Zou MX, Wang L, Lv YB, Zhou JB, Cao MR, Li YG. Analyzing the LncRNA, miRNA, and mRNA Regulatory Network in Prostate Cancer with Bioinformatics Software. J Comput Biol. 2018;25:146–57.

22.Feber A, Xi L, Luketich JD, Pennathur A, Landreneau RJ, Wu M, Swanson SJ, Godfrey TE, Litle VR. MicroRNA expression profiles of esophageal cancer. J Thorac Cardiovasc Surg. 2008;135:255–60; discussion 60.

23.Zhao BS, Liu SG, Wang TY, Ji YH, Qi B, Tao YP, Li HC, Wu XN. Screening of microRNA in patients with esophageal cancer at same tumor node metastasis stage with different prognoses. Asian Pac J Cancer Prev. 2013;14:139–43.

24.Chen H, Yang Y, Wang J, Shen D, Zhao J, Yu Q. miR–130b–5p promotes proliferation, migration and invasion of gastric cancer cells via targeting RASAL1. Oncol Lett. 2018;15:6361–7.

25.Schmitt AM, Chang HY. Long Noncoding RNAs in Cancer Pathways. Cancer Cell. 2016;29:452–63.

26.Han W, Liu J. LncRNA-p21 inhibited the proliferation of osteosarcoma cells via the miR–130b/PTEN/AKT signaling pathway. Biomed Pharmacother. 2018;97:911–8.

27.Ling H, Fabbri M, Calin GA. MicroRNAs and other non-coding RNAs as targets for anticancer drug development. Nat Rev Drug Discov. 2013;12:847–65.

28.Xiong Z, Ren S, Chen H, Liu Y, Huang C, Zhang YL, Odera JO, Chen T, Kist R, Peters H, et al. PAX9 regulates squamous cell differentiation and carcinogenesis in the oro-oesophageal epithelium. J Pathol. 2018;244:164–75.

29.Tan B, Wang J, Song Q, Wang N, Jia Y, Wang C, Yao B, Liu Z, Zhang X, Cheng Y. Prognostic value of PAX9 in patients with esophageal squamous cell carcinoma and its prediction value to radiation sensitivity. Mol Med Rep. 2017;16:806–16.

30.Lee JC, Sharma M, Lee YH, Lee NH, Kim SY, Yun JS, Nam SY, Hwang PH, Jhee EC, Yi HK. Pax9 mediated cell survival in oral squamous carcinoma cell enhanced by c-myb. Cell Biochem Funct. 2008;26:892–9.

Table

Table 1. Primer sequences for RT-qPCR.

Gene	Primer sequence
DIO3OS	Forward: 5'-ATACCTACCCCTCCCCAACT-3'
	Reverse: 5'-TACCTGCTCTGAGATGTGCC-3'
miR-130b	Forward: 5'-GCGGCGGCAGTGCAATGATGAAAG-3'
	Reverse: 5'-ATCCAGTGCAGGGTCCGAGG-3'
PAX9	Forward: 5'-TGCTGGACATGGGTGGCA-3'
	Reverse: 5'-AGGCAGAAGGGTTGGAGGG-3'
GAPDH	Forward: 5'-GGGCCAAAAGGGTCATCATC-3'
	Reverse: 5'-ATGACCTTGCCCACAGCCTT-3'
U6	Forward: 5'-CTCGCTTCGGCAGCACA-3'
	Reverse: 5'-AACGCTTCACGAATTTGCGT-3'

Notes: RT-qPCR, reverse transcription quantitative polymerase chain reaction; miR-130b, microRNA-130b; PAX9, paired box 9; GAPDH, glyceraldehyde-3-phosphate dehydrogenase

Figures

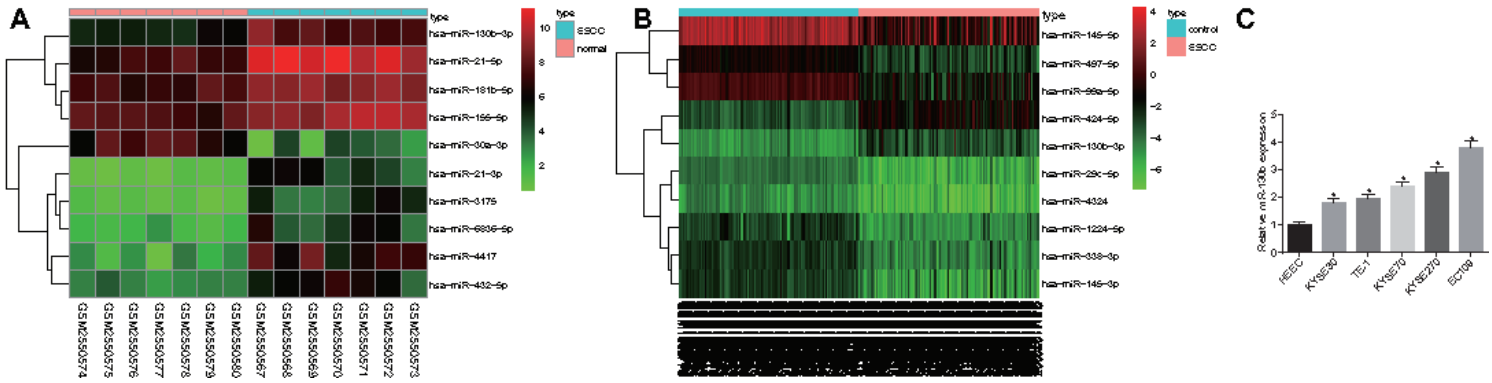

Figure 1

miR-130b expresses at a high level in ESCC and associates with poor survival rate. A and B, The heatmaps of the top 10 differentially expressed miRNAs of GSE97049 and GSE43732 where the X axis indicates the sample number, the Y axis indicates the differentially expressed miRNA, and the right upper histogram is color scale, each rectangle corresponds to expression of a sample. C RT-qPCR detection of the relative expression of miR-130b in ESCC cell lines, * $p < 0.05$ versus HEEC cell line. Data were depicted in mean ± standard deviation. The paired t test was used for comparison between the ESCC tissue and adjacent normal tissue, and one-way ANOVA followed by Tukey's post hoc test for comparison among multiple groups. The experiment was independently repeated 3 times.

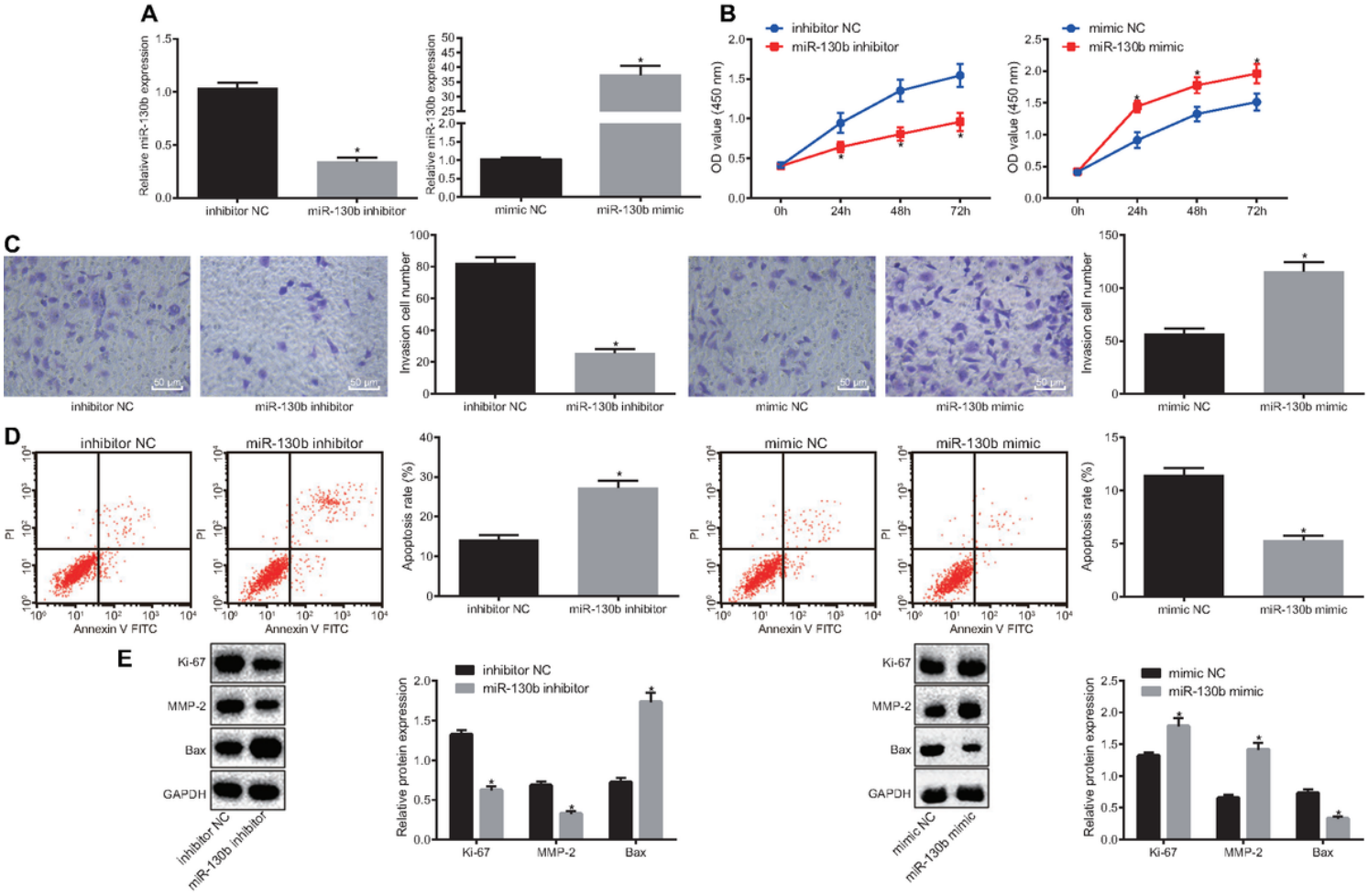

Figure 2

Upregulated miR-130b promotes the proliferation and invasion and hampers the apoptosis of ESCC cells. A, RT-qPCR to evaluate the efficiency miR-130b mimic or inhibitor in EC109 cells. B, CCK-8 to detect the effect of miR-130b on EC109 cell proliferation in response to miR-130b inhibitor or miR-130b mimic. C, Transwell assay to detect the effect of miR-130b on EC109 cell invasion in response to miR-130b inhibitor or miR-130b mimic (× 200). D, Flow cytometry to detect the effect of miR-130b on EC109 cell apoptosis in response to miR-130b inhibitor or miR-130b mimic. E, Western blot analysis to detect the effect of miR-130b on the expression of Ki67, MMP-2 and Bax in the EC109 cells in response to miR-130b inhibitor or miR-130b mimic. * $p < 0.05$ versus the inhibitor NC group, # $p < 0.05$ versus the mimic-NC group. Data were depicted in mean ± standard deviation. The independent sample t test was used for comparison between two groups, and repeated measures ANOVA for comparison at different time points. The experiment was independently repeated 3 times.

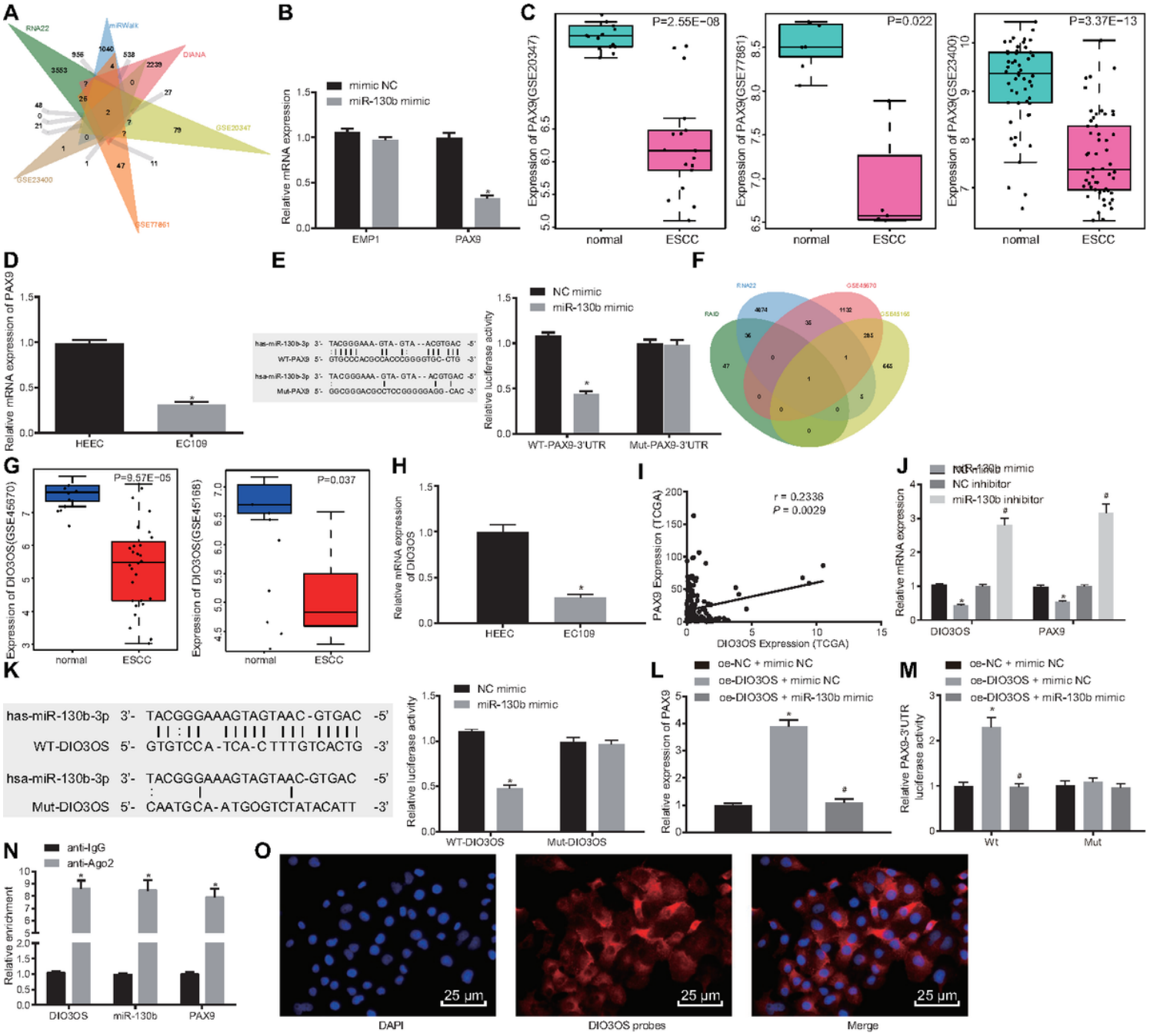

Figure 3

DIO3OS upregulates the expression of PAX9 by interacting with miR-130b. A, Comparison of the prediction results in the RNA22, miRWalk and DIANA databases with the differentially expressed genes obtained from GSE20347, GSE77861 and GSE23400. B, RT-qPCR to detect the effect of miR-130b on expression of EMP1 and PAX9, * $p < 0.05$ versus the mimic NC group. C, The expression of PAX9 in GSE20347, GSE77861 and GSE23400. D, RT-qPCR to detect the expression of PAX9 in ESCC cells, * $p < 0.05$ versus the HEEC cell line. E, The putative binding sites of miR-130b and PAX9 predicted by biological website, and the determination of luciferase activity by dual luciferase reporter gene assay, * $p < 0.05$ versus the mimic NC group. F, Comparison of the prediction results in the RAID and RNA22 databases with the differentially expressed lncRNAs obtained from GSE45670 and GSE45168. G, The expression of

DIO3OS in GSE45670 and GSE45168, respectively. H, RT-qPCR to detect the expression of DIO3OS in ESCC cells, * p < 0.05 versus the HEEC cell line. I, The expression of DIO3OS and PAX9 in 161 ESCC tissues in TCGA database. J, RT-qPCR to detect the effect of miR-130b on the expression of DIO3OS and PAX9 in cell experiments, * p < 0.05 versus the mimic NC group. # p < 0.05 versus the NC inhibitor group. K, The putative binding sites of miR-130b and DIO3OS predicted by biological website, and the determination of luciferase activity by dual luciferase reporter gene assay, * p < 0.05 versus the mimic NC group. L, RT-qPCR to detect the expression of PAX9 in EC109 cells. * p < 0.05 versus the oe-NC + mimic NC group. # p < 0.05 versus the oe-DIO3OS + mimic NC group. M, Dual-luciferase reporter gene assay to assess the luciferase activity of wt-PAX9 3'-UTR and mut-PAX9 3'-UTR. * p < 0.05 versus the oe-NC + mimic NC group. # p < 0.05 versus the oe-DIO3OS + mimic NC group. N, RIP assay to detect the binding of DIO3OS, miR-130b or PAX9, * p < 0.05 versus the anti-IgG group. O, RNA-FISH to detect the cellular localization of DIO3OS expression in EC109 cells (× 400, scale bar = 25 μm). Data were depicted in mean ± standard deviation. The independent sample t test was used for the comparison between two groups, and one-way ANOVA was used for the comparison among multiple groups. The experiment was independently repeated 3 times.

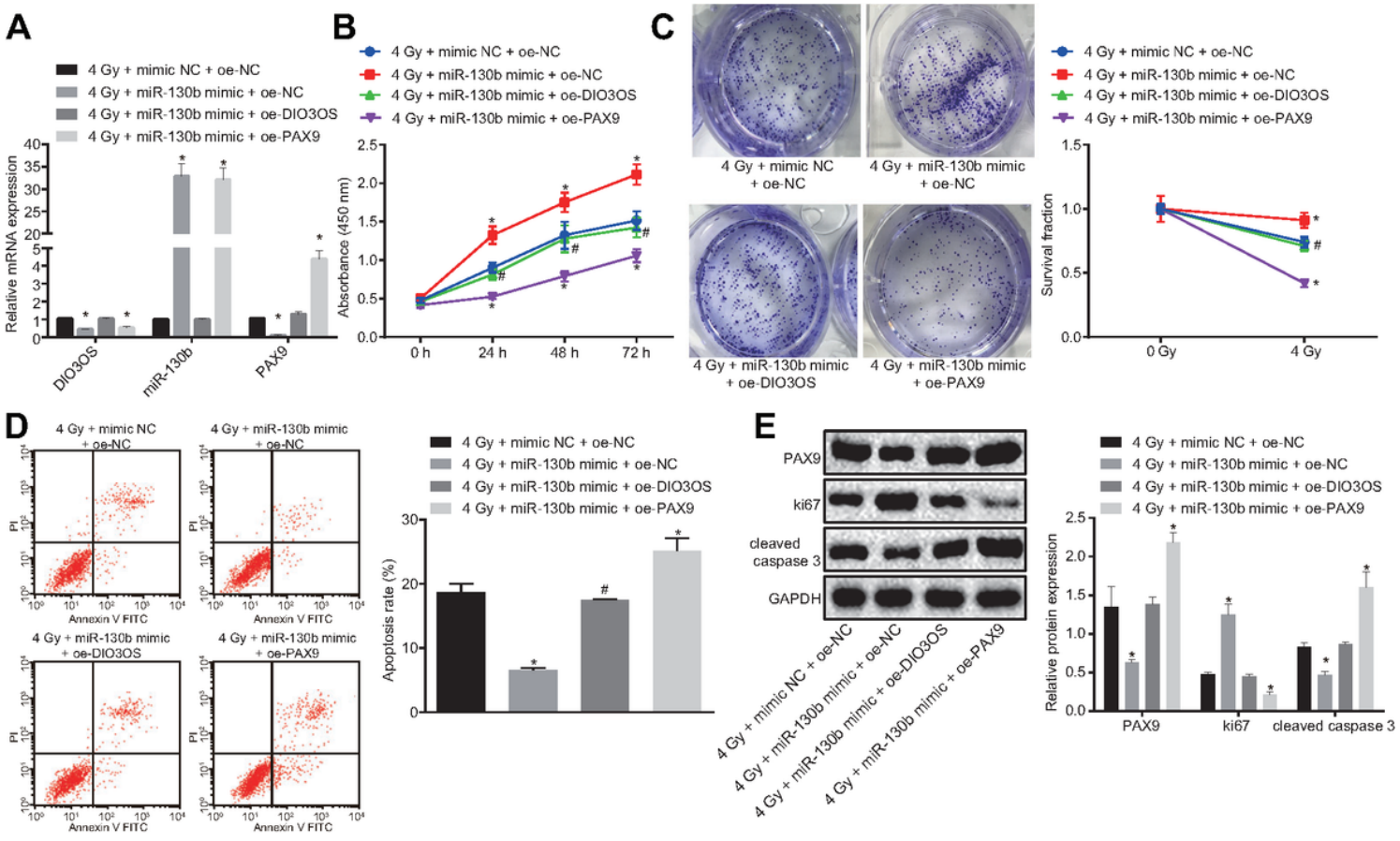

Figure 4

DIO3OS and PAX9 can reverse the effect of miR-130b on the sensitivity of ESCC to radiotherapy. A, RT-qPCR to detect transfection efficiency of oe-DIO3OS, miR-130b mimic and oe-PAX9 in EC109 cells. B, CCK-8 assay to detect the viability of transfected EC109 cells receiving 4 Gy radiation. C, Colony formation assay to detect the survival ability of transfected EC109 cells in response to 4 Gy radiation. D,

Flow cytometry to detect the apoptosis rate of transfected EC109 cells receiving 4 Gy radiation. E, Western blot analysis to detect expression of PAX9, Ki67 and cleaved caspase-3 in transfected EC109 cells in response to 4 Gy radiation. * $p < 0.05$ versus the 4 Gy + mimic-NC + oe-NC group, # $p < 0.05$ versus the 4 Gy + miR-130b mimic + oe-NC group. Data were depicted in mean ± standard deviation. The independent sample t test was used for comparison between two groups, and repeated measures ANOVA followed by Tukey's post hoc test was utilized for comparison among multiple groups at various time points. The experiment was independently repeated 3 times.

Figure 5

DIO3OS and PAX9 can subvert the effect of miR-130b on radiosensitivity of ESCC in vivo. The nude mice were injected with LV-sh-miR-130b, LV-oe-miR-130b, LV-oe-DIO3OS and LV-oe-PAX9 alone or in combination in response to 4 Gy radiation. A, Quantitation of volume of transplanted tumors. C, Quantitation of weight and representative images of transplanted tumors. C, Western blot analysis to detect expression of Ki67, cleaved caspase3 and PAX9 in transplanted tumors. D, Immunohistochemistry to observe the expression of Ki67 and cleaved caspase3 (× 400). * $p < 0.05$ versus the 4 Gy + LV-sh-NC group. # $p < 0.05$ versus the 4Gy + LV-oe-NC. & $p < 0.05$ versus the 4Gy + LV-oe-miR-130b group. Data were depicted in mean ± standard deviation. The independent sample t test was used for comparison between two groups, and repeated measures ANOVA for comparison at different time points. n = 12. The experiment was independently repeated 3 times.

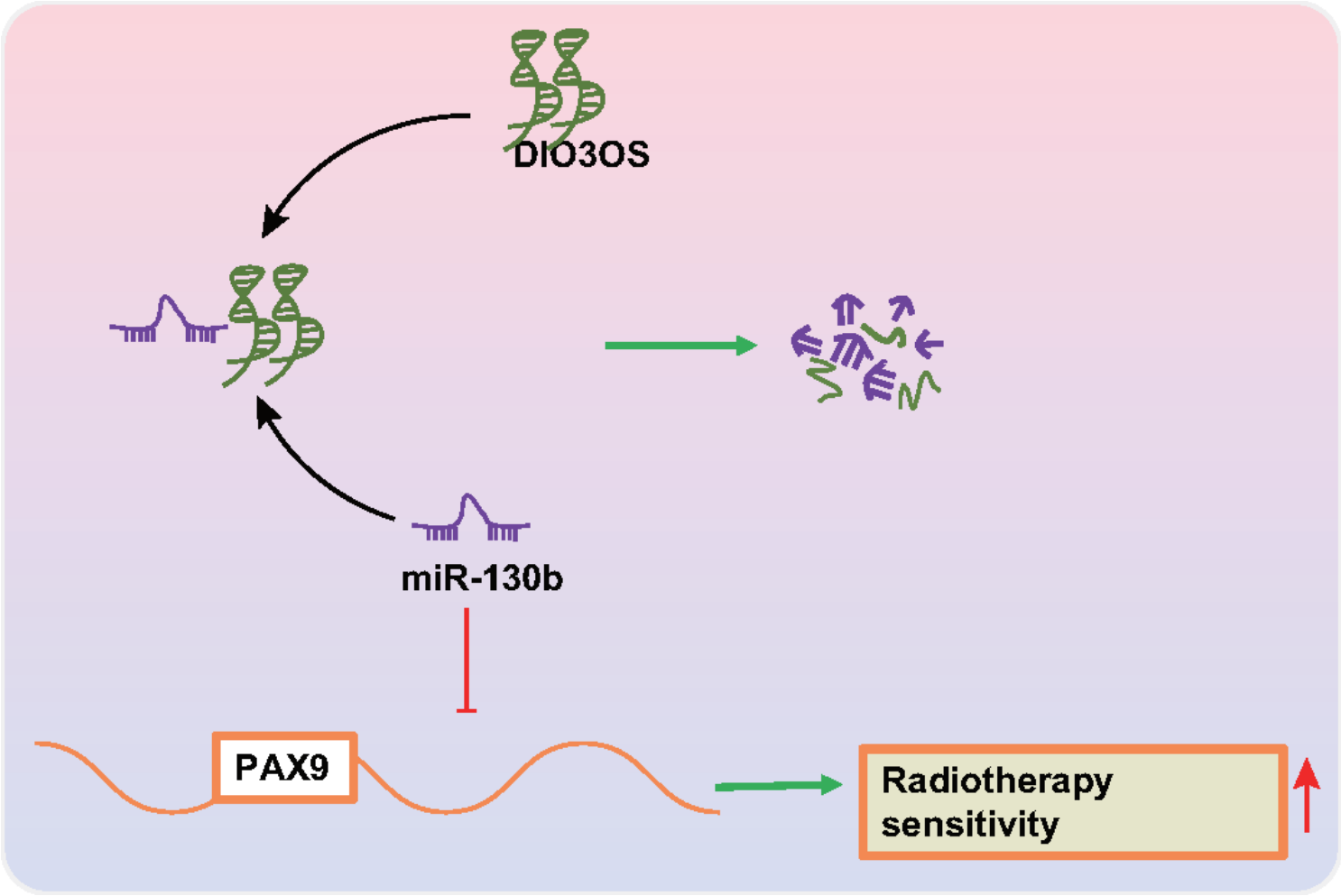

Figure 6

The schematic representation of the DIO3OS/miR-130b/PAX9 axis in radiosensitivity of ESCC. DIO3OS upregulates PAX9 by binding to miR-130b, whereby overexpression of DIO3OS could improve the radiosensitivity of ESCC.

Supplementary Files

This is a list of supplementary files associated with this preprint. Click to download.

- FigureS2.eps
- FigureS1.eps
- Supplementaryfigurelegends.docx